A model chain approach for coastal inundation: Application to the bay of Alghero

A model chain approach for coastal inundation: application to the bay of Alghero

Matteo Postacchini[a,*], Francesco Lalli[b], Francesco Memmola[a], Antonello Bruschi[b], Debora Bellafiore[c], Iolanda Lisi[b], Gianluca Zitti[a], Maurizio Brocchini[a]

[a] *Department of Ingegneria Civile, Edile e Architettura, Università Politecnica delle Marche, Ancona, Italy*
[b] *ISPRA, Istituto Superiore per la Protezione e la Ricerca Ambientale (Rome, Italy)*
[c] *Institute of Marine Sciences-National Research Council (ISMAR-CNR), Castello 2737/F (Venice, Italy)*

Abstract

Coastal inundation is an important threat for many nearshore regions worldwide, and has significantly increased in the last years also due to sea-level rise and augmented impact of extreme events, like sea storms. Many countries and regions have recently invested to overcome such problems, which commonly lead to structure damages, beach erosion and many other consequences. Numerical modeling is an important tool for coastal inundation prediction, being a valuable support for management issues to mitigate the inundation risk or suggest resilient solutions. The present work illustrates a novel approach, based on a numerical model chain that exploits a tide-surge-wave operational modeling system (Kassandra), a phase-averaged model (ROMS-SWAN) for the wave propagation towards the shore, and a phase-resolving solver (NSWE) for the prediction of runup and coastal inundation. Such a chain is applied to the bay of Alghero (Sardinia, Italy), where the results of the mentioned chain are compared to those obtained using, in place of the phase-averaged model, an analytical model for the wave propagation. Results confirm that both chain approaches provide comparable inundations, though the use of the analytical, more approximate (e.g., less accurate and reliable description of wave breaking dissipation), model suggests more severe conditions and larger flooded areas. Our contribution provides a methodological approach for an accurate and reliable estimate of coastal flooding.

Keywords: coastal flooding, coastal regulation, numerical model chain, NSWE, SWAN-ROMS, Kassandra

*Corresponding author
Email address: m.postacchini@staff.univpm.it (Matteo Postacchini)

1. Introduction

Inundations due to sea storms may generate significant problems for coastal communities, in terms of potential damages to engineering works and recreational activities, but also environmental issues. Coastal flooding could be induced by several physical phenomena (e.g., see Weisse et al., 2014; Di Risio et al., 2017) such as river flooding, tides (considering both meteorological and astronomical components), sea storms (e.g., waves running up the coast). The effects of the floodings could be even worsened by the combination of all of them. Moreover, erosion phenomena are intimately related to flooding events and may worsen the threat. In this context, even the effects of climate change, mainly in terms of sea-level rise, are thought to induce worldwide increasing exposure levels to storm events in the long period (e.g., Perini et al., 2016). Furthermore, some studies highlight that climate changes may also induce an increase in sea storminess, and consequently in coastal inundations frequency (CCCuk, 2016; Barcikowska et al., 2018; Helman and Tomlinson, 2018).

The literature review reveals that there are uncertainties inherent in the runup estimation that can affect flooding results. First, the computational procedure should be developed by taking into account detailed information about the local wave climate, with specific focus on seasonal behavior and fluctuations (De Leo et al., 2018). It is necessary to choose representative storm conditions, through an analysis of measured waves and water level time series, in order to generate maximum water level scenarios with different return periods (e.g., Salecker et al., 2011; Corbella and Stretch, 2012; Villatoro et al., 2014).

Once the storm forcing is selected, it is important to simulate its propagation towards the coast with an appropriate spatial and temporal resolution. Such procedure implies that wave conditions have to be first propagated towards the shore to evaluate shallow-water parameters and afterwards to compute runup accordingly, leading to more reliable runup expected value estimates in the case of extreme events (Di Risio et al., 2017; De Leo et al., 2018). In order to assess the potentially flooded areas related to specific storm conditions, the main parameter to be considered is the runup, defined as the seawater upper limit reached at a shoreline (de la Peña et al., 2012). Different approaches can be used for runup estimation. Empirical approaches are based on models like that proposed by Stockdon et al. (2006) combined with the berm or dune heights of a shore to achieve its runup vulnerability. However, Stockdon et al. (2006)'s formulation intrinsically leads to a very conservative result, as it provides a value linked to the 2% probability of exceedance. Therefore, evaluation of high return period runup values could lead to highly overestimated coastal vulnerability, as the return period is closely tied to the probability of non exceedance (De Leo et al., 2018).

It is also possible to use numerical models, based on physical conservation laws, to simulate the propagation of each single wave towards the coast and its runup on the emerged beach. Of great relevance are the approaches based on shallow water equations through deterministic Boussinesq models or stochastic Reynolds-Averaged Navier-Stokes (RANS) models (Cavaleri et al., 2007).

In recent years, local Authorities are showing an increasing attention to studies aimed to identify the most critical areas of flooding and to determine the most effective methodologies to address the selection of mitigation measures, both structural and non-structural (Heidari, 2009). In this context, the implementation of numerical models is important to predict inundation levels and to select the protection standards needed (e.g., De Girolamo et al., 2017).

In view of the above, this paper proposes a methodology to carry out high resolution numerical studies to characterize the flooding produced by sea waves in terms of runup, set-up, storm surge and tides, while river floodings, coastal erosion and climate changes are not taken into account. In more detail, the present study aims at coupling a series of numerical models and systems to reproduce the marine hydrodynamics from the offshore to the coast. The methodology is based on the use of either the recordings of an offshore-located buoy or the output of a tide-surge-wave forecasting system (e.g., Ferrarin et al., 2013; Mentaschi et al., 2015). In the last decades, a large number of operational systems have been implemented, like the SHYFEM Model for detecting, among other processes, high tides in the Venice Lagoon (Zampato et al., 2016), and the Kassandra storm surge forecasting system (Ferrarin et al., 2013).

Then, such offshore data need to be transferred shoreward before running a phase-resolving-model (PRM hereafter) simulation, this mainly describing the onshore wave propagation in intermediate/shallow waters and the swash-zone dynamics. Hence, another model is needed to provide such transfer from the offshore to the nearshore region. This can be either a phase-averaged model (PAM hereafter), like a circulation model (e.g., ROMS) coupled with a wave-propagation model (e.g., SWAN) or SHORECIRC (e.g., Haas and Warner, 2009; Russo et al., 2013), or an analytical model (AM hereafter), like that proposed by Goda (2010). Therefore, while the PRM typically handles $O(1\times1)\text{km}^2$ domains, the PAM and AM are concerned with larger-scale domains, i.e. $O(10\times10)\text{km}^2$. PAMs can also be used for a rough estimate of the wave runup, as they can provide the (phase-averaged) lower boundary of the swash zone.

Finally, the PRM exploits the output from the intermediate model, i.e. either PAM or AM, as the boundary condition necessary to propagate the waves from intermediate/shallow waters up to the shore, and investigate the inundation in the time domain. High-resolution PRMs for the detailed description of the nearshore wave-induced flow are of different kinds and nature, depending on the solving equations and the approach used for their solution. Typical numerical solvers suitable for the nearshore hydrodynamics can be classified as follows:

- Nonlinear Shallow Water Equation (NSWE hereafter) models, like those described by, e.g., Brocchini et al. (2001); Briganti et al. (2016);
- Boussinesq models (e.g., Kennedy et al., 2000);
- non-hydrostatic models (Ma et al., 2012; Antuono and Brocchini, 2013; Antuono et al., 2017).

Next to the description of the proposed methodology, the paper illustrates an application for the Alghero bay (Sardinia, Italy). In Section 2, the proposed

methodology, i.e. the structure of the modeling chain, is illustrated. Section 3 details the Alghero-bay area and the available data, then describes the application of the methodology to such site. Results and discussion are presented in Section 4. Some conclusions close the paper (Section 5).

2. The modeling chain: methodology

The methodology used to couple the different models is illustrated in the followings. First of all, the offshore datum is retrieved, then it is used for an intermediate propagation, using either a phase-averaged or an analytical model. Then, after a suitable generation of boundary conditions, a phase-resolving model is used, as the final step, to get the beach inundation. A scheme of the modeling chain is reported in Figure 1.

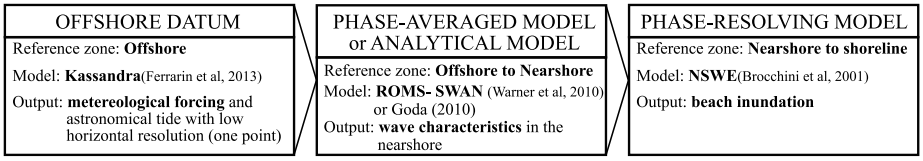

Figure 1: Scheme of the modeling chain.

2.1. The offshore datum

In the modeling chain proposed in this work, the Kassandra system has been used to generate the offshore datum. Kassandra is an operational system for storm-surge forecast on the Mediterranean and Black Seas (Ferrarin et al., 2013). It is based on a 3D finite-element hydrodynamic model that also reproduces astronomical tides, coupled to a third generation unstructured wave model. The system accounts for several interactions among wave, surge and tide, such as the wave contribution to the total water level by means of wave setup, the influence of tide and surge on the water depth, the depth and current refraction of waves by surge water level and currents. The finite-element method permits to follow the details of bathymetry and morphology in the coastal zone, describing the areas of special interest with higher resolution.

The forecast system implemented over the Mediterranean Sea runs on an unstructured grid of about 140000 elements, with variable horizontal resolution from 15km to 1km, from offshore approaching the coast. The system provides daily forecasts, to maximum 4 days each, at steps of 3 hours for the total water level (tide + surge + wave set-up) and significant wave height, period and direction. The meteorological forcing is supplied by a high-resolution meteorological model chain implemented at CNR-ISAC (National Research Council of Italy - Institute of Atmospheric Sciences and Climate) with a daily operational system[1]. The model framework comprises the GFS model (NOAA/NCEP,

[1] http://www.isac.cnr.it/dinamica/projects/forecasts

global, six days of forecast[2]), the hydrostatic model BOLAM (0.1-degrees resolution for the period considered, three days of forecast, implemented over the Euro-Mediterranean region and nested in GFS) and the non-hydrostatic model MOLOCH (0.021 degrees for the period considered, two days of forecast, implemented over Italy and nested in BOLAM, Malguzzi et al., 2006). The astronomical tide calculated by the global FES2004 model Lyard et al. (2006) is imposed to the hydrodynamic model as boundary condition at the Strait of Gibraltar.

For this application, a dataset covering the period 2012-2016, for the whole coast of Sardinia, is used. Such dataset comes from the MCWAF (Mediterranean Coastal WAve Forecast) system, managed by ISPRA (Inghilesi et al., 2016).

2.2. From the offshore to the nearshore region: phase-averaged modeling (PAM)

A PAM can be used to propagate the hydrodynamic forcing provided either by a buoy or by a large-scale/basin-scale model at significant water depths and distances from the coast. This may be a circulation model like ROMS, where the contribution of short waves appears in the momentum equation in the form of Radiation Stress tensor once their characteristics are known (e.g. from a coupled wave driver). This, together with an appropriate spatial and temporal resolution, enables the hydrodynamics reconstruction in large coastal regions.

The first step consists in the choice of the offshore boundary condition for the PAM. If a wave buoy is available, the offshore boundary of the PAM should be as close as possible to its location. Conversely, if the climate of the basin is reconstructed using a large-scale model, the location of the PAM boundary should adapt to one or more grid points of the large-scale model. Hence, data suitability should be checked, especially in the nearshore region, where coast-induced shading effects may occur. Use of grid points sufficiently far from gulfs or bays is thus suggested.

The information to be used as PAM boundary condition depends on the scope of the study at hand. This may represent a wave with a required return period (e.g. $T_R = 2$ years), or a specific, actually occurred, sea storm. Actions like currents, tide or residual levels can also be included in the boundary condition.

With the aim to fulfill numerical stability, the model is initialized with a "spin-up" run, during which the domain is subjected to a small wave forcing, to be as close as possible to the wave characterizing the very beginning of the boundary condition of the actual simulation. Once steadiness is reached, the result obtained from the spin-up run throughout the domain is used as the initial condition for the actual simulation.

The resolution of the PAM grid depends on the selected domain, i.e. its size, the complexity of the reproduced bathymetry and the characteristics (duration, peak heights, etc.) of the chosen sea storm or sea state. Hence, it would be appropriate to re-size the spatial and temporal resolutions depending on a long-lasting simulation (resolution decrease), rather than on large bathymetric gradients (resolution increase). Once the grid is set up, the bathymetry

[2] http://www.emc.ncep.noaa.gov/GFS

needs to be generated exploiting all available datasets. Since close to the shore, high-resolution surveys are performed, while a lower resolution characterizes both emerged regions and offshore areas, an appropriate interpolation of such data must be undertaken, hence preferring higher-resolution datasets in the overlapping areas. To improve the obtained interpolation and remove spurious gradients (e.g., due to the overlapping of datasets of different nature), a regularization or slight smoothing of the resulting bathymetry can be undertaken. It is difficult to provide a general rule for such smoothing. However, it should be weak enough to avoid major alterations of the hydrodynamics and runup.

Once the simulation is ended, the numerical results are used as inputs for the PRM, in terms of both boundary and initial conditions. In more detail, a small portion of the bathymetry exploited for the PAM simulation is used for the generation of the higher-resolution PRM grid. Furthermore, the hydrodynamic outputs of the PAM simulations are extracted at the location where the offshore boundary of the PRM domain is set, with the aim to provide the boundary condition for the PRM simulations.

For the present analysis, the circulation model ROMS and the wave driver SWAN (ROMS-SWAN hereafter) have been coupled within COAWST (Coupled Ocean-Atmosphere-Wave-Sediment Transport modeling system, Warner et al., 2010) in order to model the nearshore dynamics. The ocean model ROMS belongs to the general class of free surface, terrain-following numerical models that solve the three-dimensional RANS equations using the hydrostatic and Boussinesq approximations (Shchepetkin and McWilliams, 2005; Haidvogel et al., 2008; Shchepetkin and McWilliams, 2009). The SWAN model (Booij et al., 1999) is a phase-averaged, third generation spectral wave model, specifically designed for shallow waters, and solves the action balance equation in either stationary or non-stationary mode (Holthuijsen, 2010).

2.3. From the offshore to the nearshore region: analytical modeling (AM)

As an alternative to the numerical modeling to transfer waves from the offshore to the nearshore shallow waters, simple analytical models may be used. An example is the approach illustrated by Goda (2010) (Go10 hereafter), which enables the estimate of both height and direction of the wave approaching the shore from deep waters (significant wave height $H_{s,0}$, peak period T_p, direction θ_0) to shallower waters (significant wave height H_s, the same peak period T_p, direction θ), in an ideal domain where obstacles or significant unevennesses like submerged bars are absent. The mechanisms that need to be accounted for are:

- **refraction**, which provides a change in both direction and wave height due to the non-parallelism of the wave fronts to the shoreline;
- **shoaling**, which provides an increase of the wave height as a consequence of the depth decrease;
- **breaking**, which provides a wave-height decrease due to the too small water depth.

The Go10 model, where a constantly sloping beach is assumed, has been used in the present application for the wave propagation from the offshore to the coast, with the aim to compare the coastal inundation obtained using simplified solutions, like Go10, with that obtained using more complex propagation models, like ROMS-SWAN. First, shoaling and refraction are described, respectively, by the coefficients K_s and K_r, which are functions of the relative water depth $h/L_{p,0}$, where h is the water depth at the target location and $L_{p,0}$ is the deep-water peak length of the irregular wave (see the specific charts reported in Go10). Further, K_r and the incidence angle of waves at the target location θ are also functions of the incident deep-water angle θ_0. Such approach, based on nonlinear shoaling, does not provide any increase of the wave energy density, but a deformation of the wave profile, i.e. a crest steepening and a trough flattening.

The breaking mechanism is accounted for by means of three parameters (β_0, β_1 and β_{max}), which depend on both deep-water wave steepness $H_{s,0}/L_{p,0}$ and seabed slope i:

$$H_s = K_r \left\{ \min \left[(\beta_0 H_{s,0} + \beta_1 h), \beta_{max} H_{s,0}, K_s H_{s,0} \right] \right\}, \quad (1)$$

$$\theta = f(\theta_0; h/L_{p,0}). \quad (2)$$

This process allows one to find the wave characteristics at the target location, i.e. H_s, T_p (constant between the offshore and the inshore) and θ, these experiencing refraction, shoaling and breaking when traveling from deep waters, where the wave characteristics are provided by, e.g., a buoy or a wave forecasting system, to finite-depth waters. If the wave data are provided in finite-depth waters, a reverse shoaling to deep waters is first needed (see Go10).

2.4. The nearshore region: boundary condition for the phase-resolving model (PRM)

Typical PRMs require the instantaneous evolution of the water flow. In the case of shallow-water models, like the NSWE solver described by Brocchini et al. (2001), the time series of free surface level and depth-averaged velocity are needed at the offshore boundary. Hence, the available wave characteristics, obtained from either PAM or AM, must be elaborated to obtain such time series.

The first step is the representation of the sea-wave conditions in the region of interest by means of a suitable spectrum, e.g. JONSWAP, which can be easily reconstructed using the available wave characteristics. The following step concerns the reconstruction of the water-level time series from the spectrum. To this aim, the procedure described by Liu and Frigaard (1999) can be used (already applied by, e.g., Postacchini et al., 2016):

1. discretization of the spectrum into a finite number of frequency intervals,
2. setting of the wave parameters (e.g., amplitude, phase) characterizing each interval,
3. summation of the waves characterizing each interval.

Each group of wave characteristics (H_s, T_p, θ) represents a specific duration, since data may be collected, e.g., every hour or every three hours by buoys or forecasting systems. As a result, if a whole sea state or sea storm needs to be simulated, more than one spectrum must be used for the generation of the offshore boundary condition. Hence, more than one time series of the water level is generated. Since all such spectrum-derived series are independent, an interpolation between them is needed, with the requirement to preserve the shape and the first derivatives, e.g., using a cubic Hermite spline. Figure 2 illustrates an example of interpolation between two contiguous and independent water-level time series (light blue lines). The first of the two series, i.e. that on the left of the separation (thick dash-dotted line), is taken as it is, while the beginning of the second series is interpolated. Hence, the resulting water-level series (black dashed line) completely overlaps the former series, while the interpolation occurs for the initial 3s of the latter series.

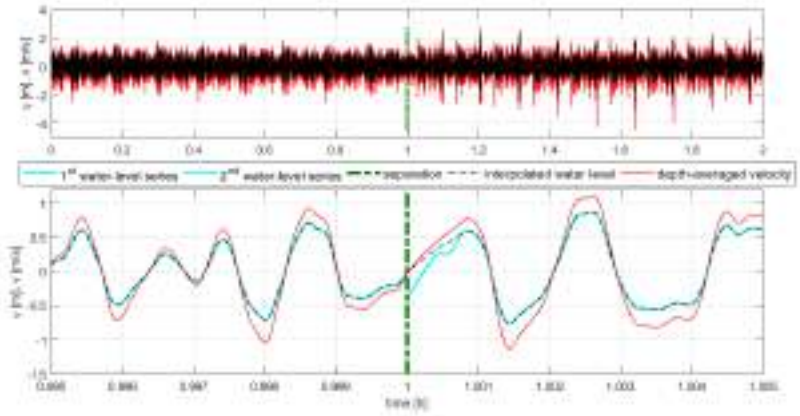

Figure 2: Example of interpolation between consecutive water-level time series: original water-level (light blue lines) and interpolated water-level (black dashed line) series. The depth-averaged velocity, reconstructed from the interpolated water level, is also illustrated (red line). Whole time series (top panel) and close-up view (bottom panel).

Finally, the associated depth-averaged flow velocity must be reconstructed. This can be done by using a suitable relationship for the shallow waters. Similarly to Zitti et al. (2016), the law proposed by Svendsen et al. (1978) and Guizien and Barthélemy (2002) can be used to estimate the depth-averaged velocity U:

$$U = \frac{c\eta}{h+\eta}, \tag{3}$$

where the phase speed is evaluated as $c = \sqrt{g(h+\eta)}$ (e.g., see Postacchini and Brocchini, 2014).

2.5. From the nearshore region to the shore: phase-resolving modeling (PRM)

Once the boundary condition is generated, the high-resolution PRM also needs an initial condition. Specifically, to be consistent with PAM runs, the PRM bathymetry should be extracted from the same datasets, but characterized by a finer grid, and should map a smaller numerical domain. Hence, the size of the computational area should be of about $(100 - 1000)$m, while the grid spacing should be around $(0.1 - 1)$m, this to allow for a detailed reconstruction of the shoreline evolution.

Such studies strictly depend on the hydrodynamics developed within the chosen domain, which, in turn, depends on the offshore boundary condition forced over the selected bathymetry/initial condition. The hydrodynamics is described in terms of water level and velocity distribution within the domain, in addition to the time series of the shoreline location, being the latter a fundamental finding for the beach inundation. As an example, a typical output is the maximum runup R_{max}, but also the value which is reached or exceeded by only two percent of the wave runups, i.e. $R_{2\%}$ (e.g., Stockdon et al., 2006).

The results of the PRM are fundamental for risk analyses of coastal regions. Specifically, for hazard mapping purposes, the inundation can be evaluated using a threshold for the water level, so as to take as flooded only those submerged regions characterized by significant water depths (order of centimeters or more). Such a value is imposed as a function of: i) the errors that characterize the topographic-bathymetric data, ii) the interpolation procedures for the grid generation, iii) the vulnerability of the site, iv) the existence of vertical elements that cannot be easily described (e.g., sidewalk, stairs), v) percolation. Hence, a threshold in the range $d_{flood} = (0.01 - 0.1)$m is suggested, which means that regions where the water depth $d < d_{flood}$ are not taken as flooded.

The NSWE solver, used in the present application, is based on the solution of the Nonlinear Shallow Water Equations, obtained from depth integration of the Reynolds equations, hence properly describing the main shallow-water processes, like the wave runup (Brocchini et al., 2001). The NSWE system in non-conservative form is:

$$d_{,t} + (ud)_{,x} + (vd)_{,y} = 0, \tag{4}$$

$$u_{,t} + uu_{,x} + vu_{,y} + gd_{,x} = gh_{,x} - B_x, \tag{5}$$

$$v_{,t} + uv_{,x} + vv_{,y} + gd_{,y} = gh_{,y} - B_y, \tag{6}$$

where (x, y, z) represents the Cartesian coordinate system; $\mathbf{v} = (u, v)$ is the vector of the depth-averaged horizontal velocity; the total water depth d and the still water depth h give the surface water level $\eta = d - h$; B_x and B_y represent the friction contribution (Chezy-type law) along the horizontal directions.

Although the NSWE model has already been used and validated under different conditions (e.g., runup and shoreline motion, dynamics of the swash zone, dynamics around rigid obstacles), as described in many recent worksBrocchini et al. (2001); Soldini et al. (2012); Briganti et al. (2016); Postacchini et al. (2016), a specific test is here presented to show the NSWE capabilities. One of the experimental tests described by Roeber et al. (2010) and carried out at the

O.H. Hinsdale Wave Research Laboratory (Oregon State University), concerning a solitary wave propagating over an idealized fringing reef, is here replicated. The tested configuration includes a fore reef and a reef flat, with water depth $h = 1$m, wave amplitude $A = 0.5$m and reef slope of 1:5. The comparison of experimental data (circles) and numerical results (solid line), in terms of surface profile, is illustrated in Fig. 3 for different time instants.

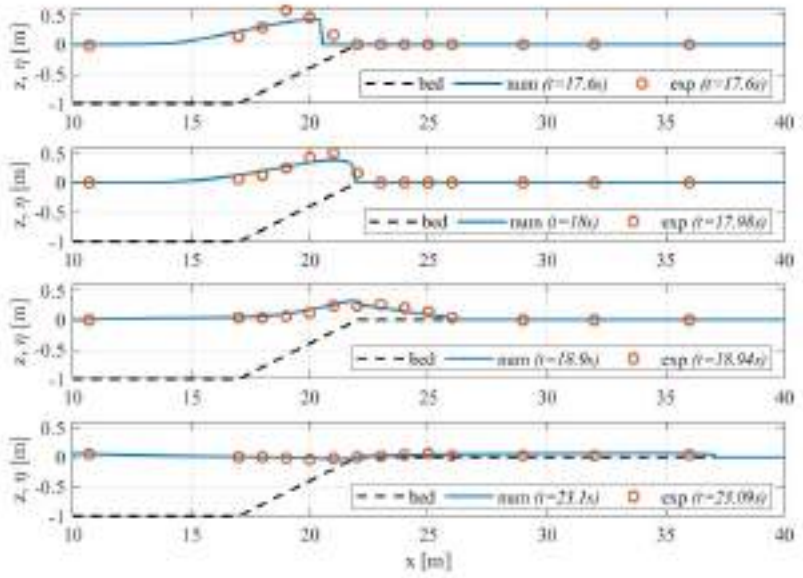

Figure 3: Comparison between Roeber et al. (2010)'s experimental data (circles) and numerical results (solid lines). The bed level (dashed lines) is also shown.

Although wave breaking occurs more offshore in the model (e.g., see the top panel of Fig. 3), as typical for NSWE-type models, the comparison between experimental data and numerical results is good, similarly to that illustrated in Roeber et al. (2010), where a Boussinesq-type (dispersive) model was used. This test confirms that the proposed NSWE model can be suitably used for the wave propagation up to the shore, thus for the estimate of beach inundation.

3. The modeling chain: an example

The aim of the present analysis is to propagate real sea storm conditions from the offshore to the emerged beach, and thus to obtain the instantaneous shoreline and the following beach inundation. To summarize what described above, the offshore data have been retrieved from the operational system Kassandra (Section 2.1). Then, the wave propagation from the offshore to the nearshore region has been undertaken using the ROMS-SWAN model (Section 2.2). Additionally to the ROMS-SWAN model, the Go10 has been applied over the

same cross-section stretch of coast (Section 2.3). The wave propagation from the nearshore to the shore has been carried out using the NSWE solver, which takes inputs from, but works independently of both ROMS-SWAN and Go10 (Section 2.5).

The complete framework of the numerical model chain is illustrated in Figure 4, where the location of the Kassandra node (blue circle), the depth used for the ROMS-SWAN domain (colored map) and the boundaries of the NSWE domains (red and green rectangles) are represented.

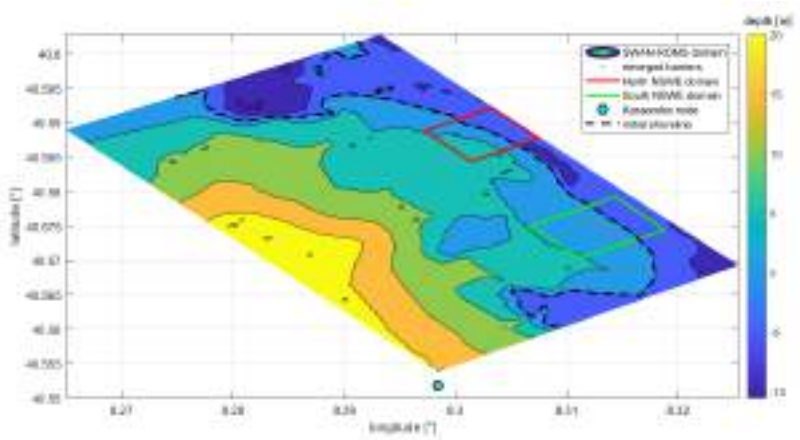

Figure 4: Bathymetry used in the ROMS-SWAN domain, Kassandra node (blue circle) and NSWE domains: North (red rectangle) and South (green rectangle) zones. The existing emerged barriers (gray dots) and the initial shoreline (black dashed lines) are also reported.

3.1. Available data

3.1.1. Site description

The site chosen for the application of the modeling chain is the bay of Alghero, located on the Northwest coast of Sardinia (Italy). Its littoral, about 5km long, is bounded by the harbor of Alghero to the South and the smaller Fertilia harbor to the North (see Figure 5).

Waves off the Alghero coast are some of the largest and more powerful experienced in Italy. The dominant wind is from the Northwest and can produce storm waves up to about 8m of significant height (APAT, 2006; Manca et al., 2013). The most frequent waves generally come from the 295°N-330°N direction and frequently are characterized by a significant height of 2m (APAT, 2006).

The seabed of the Bay is characterized by a vast Posidonia oceanica seagrass meadow, covering an area of about 13km^2 from the 5m to the 30m depth (Pala et al., 2009). Although such vegetation is important in terms of beach protection, providing large wave dissipation, and could be successfully modeled by increasing the seabed friction (see eqs. 5 and 6), a spatially homogeneous friction coefficient has been used in the present application for the sake of simplicity, and

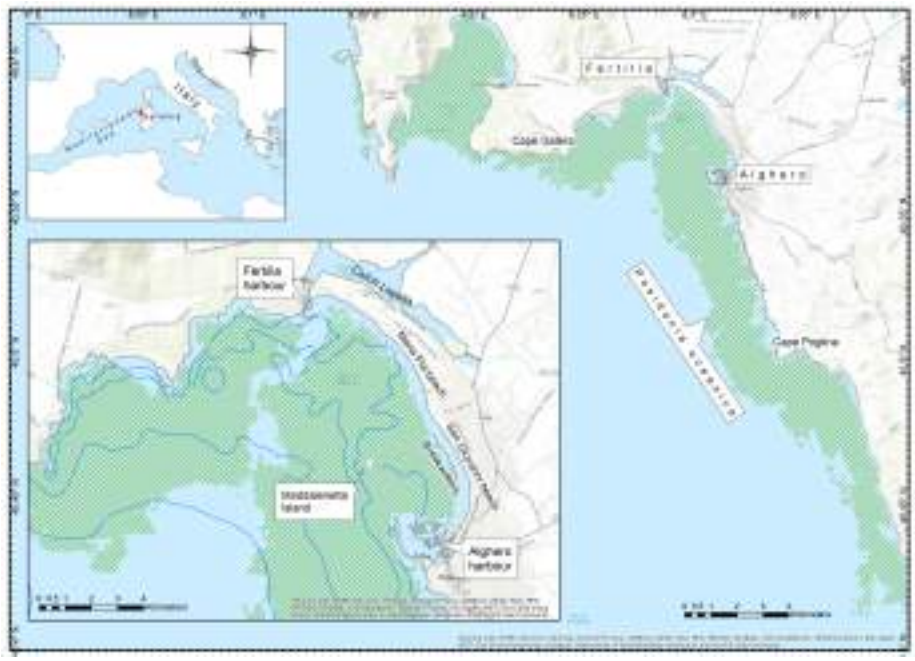

Figure 5: The Alghero bay case study, Northwest coast of Sardinia (Italy).

also because neglecting such additional dissipation contribution leads to more precautionary results. Moreover, it has also been found that Posidonia oceanica is much less efficient when subject to the large waves that are here analyzed to study coastal flooding(e.g., see Manca et al., 2012). A small rocky island (Isola della Madalenetta, see Figure 5) is located within the 5m depth contour roughly in front of Punta del Paru.

The Alghero-Fertilia littoral shows erosional trends of the shoreline and of the sandy beach, especially caused by large winter storms. Manca et al. (2013) highlight that even if the areas with shoreline accretion are slightly larger than the retreat areas, erosion phenomena occur along the shoreline in object. In particular, erosion affects the most valuable sectors of the littoral.

In the Southern sector of the bay (South of Punta del Paru), there is the urban beach of Lido San Giovanni. This area is characterized by seaside resorts and by the presence of the Alghero harbor. The expansion of the Alghero harbor led to erosion phenomena, creating a risk of flooding to the nearby coastal railway station and other coastal assets (Manca et al., 2013). Thus, near the town of Alghero, offshore breakwaters were built to protect the coast of Lido of San Giovanni beach.

3.1.2. Surge-tide-wave data

Kassandra provided the offshore dataset, covering the period 2012-2016, with time step of 3 hours. The variables computed are:

- water level, including the signal due to tidal potential, wind and atmospheric pressure (storm surge) and the wave set-up;
- 3D tidal current;
- significant wave height, wave period and direction.

The Kassandra forecasting system runs daily, covering a period of four days. In order to provide a continuous dataset, the considered data are the merge of the first forecasted day of each daily run. The following forecasted days were considered in the dataset in limited cases if data gaps were present due to stops of the forecasting systems. The dataset here used is a subset of the above mentioned variables time series, computed on the nodes of the unstructured grid in the coastal area within the bathymetry of 20m around Sardinia Island.

3.1.3. Bathymetries

Two bathymetric data sources have been used to compile the computational grid. A nested hierarchy has been used for the data, i.e. a more accurate dataset has priority over poorer quality data.

First, single-beam swath bathymetry data have been collected in January 2014 by Regione Sardegna. Surveys have been carried out using a small vessel equipped with Reson Navisound 210, i.e. an echosounder with one channel at a working frequency of 200kHz for hydrographic survey operations. Such collected data allowed the construction of the first bathymetric dataset with a resolution of 3m×3m covering approximately an area from the outer surf zone up to the shoreline.

The second dataset has been provided by the Hydrographic Institute of the Italian Navy ("Istituto Idrografico della Marina"). It is characterized by a coarser resolution and covers a larger portion of the submerged beach, i.e. up to a depth of about 30m.

3.2. The extreme event

The wave height time series extracted from the Kassandra dataset in the computational point closest to Alghero were analyzed to identify and simulate the shoreward propagation of an extreme event with a specific return period T_r (defined as the average time occurring between two events of equal intensity, higher than a specific threshold). For the present study, $T_r = 2$ years is considered.

The procedure used to identify the wave height corresponding to $T_r = 2$ years starts with the identification of the subset of extreme events of storm surge, extracting the cases characterized by a wave height higher than a given threshold (i.e. 1.5m, if the definition given by Boccotti, 1997, is followed) for a time longer than 12 hours, and values below such threshold for a time smaller than 12 hours. Two events are considered independent if their temporal distance is at least 48 hours. The extreme event analysis is then performed on the identified subset of events using the Generalized Pareto Probability Distribution (GPD) to fit the

distribution. The subset is assumed to be composed of random variables that are independent and identically distributed.

The GPD probability density function depends on three parameters, i.e. the scale s, the shape k and the threshold q. To compute the parameters that lead to the best fit, the maximum likelihood approach for k and s is chosen, once the q parameter is defined through the POT (Peak Over Threshold) methodology, and once it has been verified that the subset of extreme events above the threshold is at least composed by 20 events. This latter check was necessary because of the limited period covered by the dataset (5 years), in order to assure statistical relevance of the analysis. The automatic procedure described in Thompson et al. (2009) is used.

The simulated storm has been chosen within the dataset, used for the statistical analysis, as that characterized by a significant height at the storm peak which was the most similar to that referring to the 2-years return period. Specifically, the chosen sea storm is that occurred between 28/01/2015 and 10/02/2015 and illustrated in Figure 6.

3.3. Model setup

3.3.1. Setup of the ROMS-SWAN model

One of the first steps to be undertaken is the grid generation for the ROMS-SWAN model. Using the Lambert conformal conic projection and the Datum WGS84, a map has been generated and then a numerical domain has been selected and discretized. Specifically, the generated grid has a spatial discretization decreasing from 25m to 4m moving shoreward.

The bathymetry has been reconstructed by interpolating the two available datasets: the high-resolution dataset relevant to the most inshore areas and the low-resolution dataset for the offshore region, described in Section 3.1.3. Since ROMS exploits a terrain-following coordinate system, the bathymetry has been smoothed of the minimum amount needed for a stable computation.

The statistic analysis of the wave data has been described in Section 3.2. Based on such findings, an actually occurred storm has been chosen, with the aim to reproduce wave characteristics as close as possible to those of a wave with $T_r = 2$ years.

The actual simulation has been preceded by a spin-up simulation (wave characteristics $H_s = 0.3$m and $T_p = 3$s), which has been run until a steady condition was reached. Then, the actual simulation has been carried out using the outputs of the spin-up run as initial conditions throughout the numerical domain. Further, the 2-years return period wintertime maximum tide ($\Delta\eta_{tide} = 0.17$m) and extreme residual level ($\Delta\eta_{res} = 0.14$m), have been imposed at the offshore boundary as an additional superelevation ($\Delta\eta_{tot} = \Delta\eta_{tide} + \Delta\eta_{res} = 0.31$m) to be taken as constant during the whole simulation. The offshore boundary condition is completed with the data retrieved from the Kassandra grid point shown in Figure 4, which have been applied to the whole offshore boundary (see Figure 6).

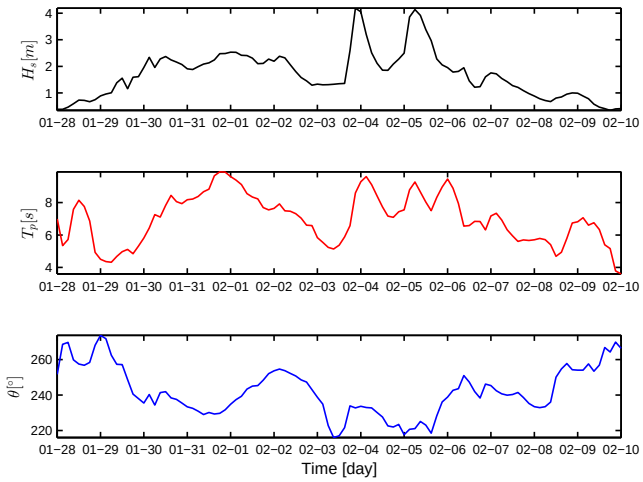

Figure 6: Time series of the main parameters used at the offshore boundary for the ROMS-SWAN simulation: H_s (top panel), T_p (middle panel) and θ (bottom panel).

3.3.2. Setup of the NSWE model

A detailed coastal inundation has been evaluated using the NSWE simulations carried out at two different locations, i.e. in the Northern and Southern parts of the Alghero bay. The bathymetries of such locations, as first illustrated in Figure 4, have been extracted from the raw bathymetry used for the coarse ROMS-SWAN simulation and then slightly smoothed using a moving average, to prevent large gradients throughout the domain. The resulting bathymetries used for the NSWE runs are shown in Figure 7 using the NSWE coordinate system, where $(x_{NSWE}, y_{NSWE}) = (0, 0)$ represents the most Southern point of each domain. The emerged breakwaters are represented by almost shore-parallel rectangles (right panel).

The numerical grid is characterized by a rectangular mesh, with spacing $(\Delta x, \Delta y) = (1, 3)$m for both cases. The domain size is (640×600)m^2 for the Northern region and (800×650)m^2 for the Southern region. The minimum depth chosen for the shoreline treatment, i.e. to distinguish between wet and dry numerical cells, is $d_{min} = 1$mm (for more details, see Briganti et al., 2012). The minimum depth, d_{min}, for wetting and drying a computational cell, is obviously different from the minimum flooding depth, which is used a-posteriori of any computation to define the flooded area.

Concerning the boundary conditions, two different types have been used: one referring to the ROMS-SWAN output at the offshore boundary location of the NSWE domains, the other referring to the Go10's wave propagation to the offshore depth of the numerical domains. For both types, a portion of the sea storm occurred between 28/01/2015 and 10/02/2015 (Figure 6), taken around the storm peak, has been propagated from the Kassandra node location (blue circle in Figure 4) to the nearshore, i.e. to the NSWE boundaries (rectangles in

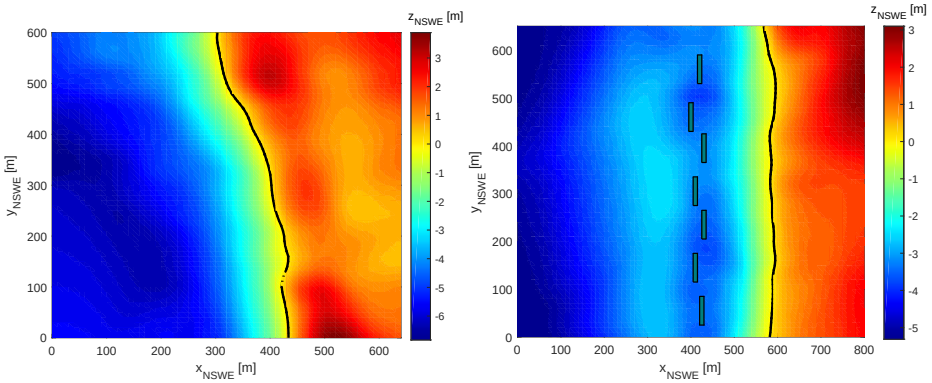

Figure 7: Numerical domains used for the NSWE simulations: Northern (left panel) and Southern (right panel) areas of Alghero bay, respectively represented in the red and green rectangles of Figure 4. The initial shoreline is also shown (black line).

Figure 4).

In particular, since the offshore/Kassandra node is located at a depth $h_{off} =$ 14.32m, in intermediate waters (since $T_p = 8.59$s, it is $h_{off}/L_p = 0.2$), and provides the wave characteristics $H_{s,Kass}$ and θ_{Kass}, a de-shoaling procedure needs to be applied for the Go10 case. Hence, waves are propagated seawards (e.g., see Stockdon et al., 2006), providing $H_{s,0}$ and θ_0, while the following shoreward propagation gives $H_{s,NSWE}$ and θ_{NSWE} at the target location, where the water depth has been chosen as $h = 4.75$m for both North and South domains (see Section 2.3). The three-hour wave characteristics related to the application of Go10's model are reported in Table 1.

Table 1: Wave characteristics transferred from the Kassandra node ($h_{off} = 14.32$m) to the NSWE offshore boundaries ($h = 4.75$m).

day/time	$H_{s,Kass}$ [m]	θ_{Kass} [°]	$H_{s,0}$ [m]	θ_0 [°]	$H_{s,NSWE}$ [m]	θ_{NSWE} [°]	T_p [s]
03.Feb.15/21:00	4.19	1.3	4.74	1.3	2.86	0.5	8.59

The wave characteristics obtained from the mentioned propagation procedures are illustrated in Table 2. All simulations include the storm peak, occurring in 03/02/2015, at 22:00. Further, the ROMS-SWAN data, provided every hour, are characterized by significantly reduced wave heights if compared to the Go10's model data, because of the rough approach used by the analytical model to represent the wave-breaking-induced energy dissipation. Since the analytical propagation is mainly based on the water depth at the target location, the wave characteristics are exactly the same at both offshore boundaries, as shown in Table 2. According to the maximum tide and residual levels, every NSWE simulation has been forced using a superelevation $\Delta\eta_{tot} = 0.31$m throughout the domain (see Section 2.2 for details).

Table 2: Wave characteristics provided by ROMS-SWAN simulations (left) and Go10's model (right) used at the offshore boundary of the Northern (top) and Southern (bottom) NSWE domains.

North	data from ROMS-SWAN			data from Go10's model		
day, time	H_s [m]	T_p [s]	θ [°]	H_s [m]	T_p [s]	θ [°]
03/02/2015, 21:00	1.97	7.16	14.72	2.86	8.59	0.50
03/02/2015, 22:00	2.30	8.10	14.72	2.86	8.59	0.50
03/02/2015, 23:00	2.18	8.10	14.72	2.86	8.59	0.50
South	data from ROMS-SWAN			data from Go10's model		
day, time	H_s [m]	T_p [s]	θ [°]	H_s [m]	T_p [s]	θ [°]
03/02/2015, 21:00	1.52	7.36	-1.51	2.86	8.59	0.50
03/02/2015, 22:00	1.64	8.10	-1.51	2.86	8.59	0.50
03/02/2015, 23:00	1.60	8.10	-1.51	2.86	8.59	0.50

The wave data of Table 2 have been used for the generation of the water level time series (Section 2.4). In the case of wave forcing from Go10's model, only a wave dataset covers the three hours, this avoiding interpolation between contiguous series. Conversely, in the ROMS-SWAN simulations, characterized by three distinct datasets, i.e. one per hour, the interpolation has been undertaken using a cubic Hermite spline (see also Section 2.4 for more details).

An example of wave propagation in the surf and swash zone in the Northern area (see the red box in Fig. 4) is illustrated in Fig. 8. Waves generated at the offshore boundary (left) starts with an angle and propagate towards the beach (right), assuming an almost shore-parallel direction. The steepest ones represent breaking waves. The intersection between the water surface (blue-green map) and the seabed (orange-red symbols) is the shoreline and describes the instantaneous beach inundation.

4. Results and discussion

4.1. The ROMS-SWAN results

Figures 9, 10 and 11 illustrate, respectively, the wave-height, wave-length and barotropic velocity results few minutes after the simulation start, when the offshore wave height is $H_s \cong 0.35$m (left panels), and at the time of maximum wave height in the domain, when the offshore wave height is very similar to the one with $T_r = 2$ years (right panels). The waves propagate through the domain, being affected by both bed morphology and coastline characteristics. The barotropic velocity is characterized by two main clockwise circulations, one around the "Maddalenetta island" (white spot within the domain), and the other one next to the North part of the coastline (right panel of Figure 11).

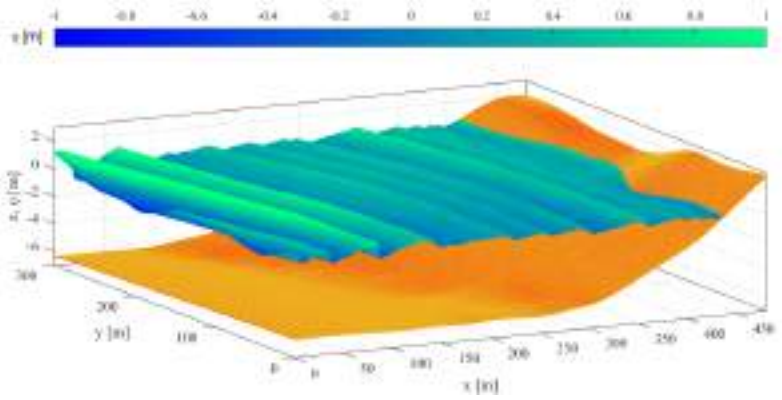

Figure 8: Example of wave propagation in a portion of the Northern area of Alghero bay: water surface elevation and seabed.

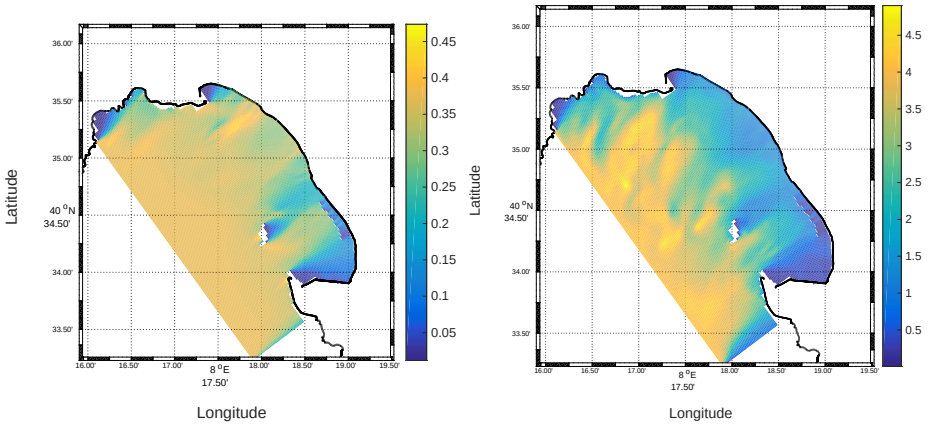

Figure 9: Significant wave height H_s at the beginning of the simulation (left panel) and at the time of maximum wave height in the domain (right panel). The shoreline is also shown (black line).

Further, Figures 10 and 11 illustrate, respectively, the wavelength L_p and the depth-averaged velocity obtained at the simulation start (left panel) and at the time of maximum wave height in the domain (right panel).

4.2. NSWE forced by ROMS-SWAN

The results of the simulations forced using the ROMS-SWAN outputs are described in the following. Some numerical gauges have been placed within the domain, mainly to track the shoreline evolution at specific alongshore locations $y = y_{NSWE}$. Figures 12 and 13 illustrate the water surface evolution η at the offshore boundary (top panels), the horizontal shoreline evolution (middle panels) or inundation x_s, and the vertical evolution or runup z_s (bottom panels).

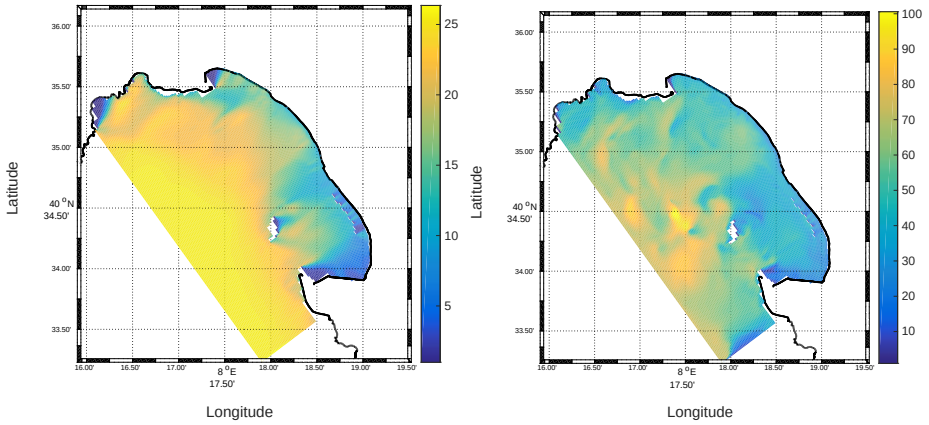

Figure 10: Peak wave length L_p at the beginning of the simulation (left panel) and at the time of maximum wave height in the domain (right panel). The shoreline is also shown (black line).

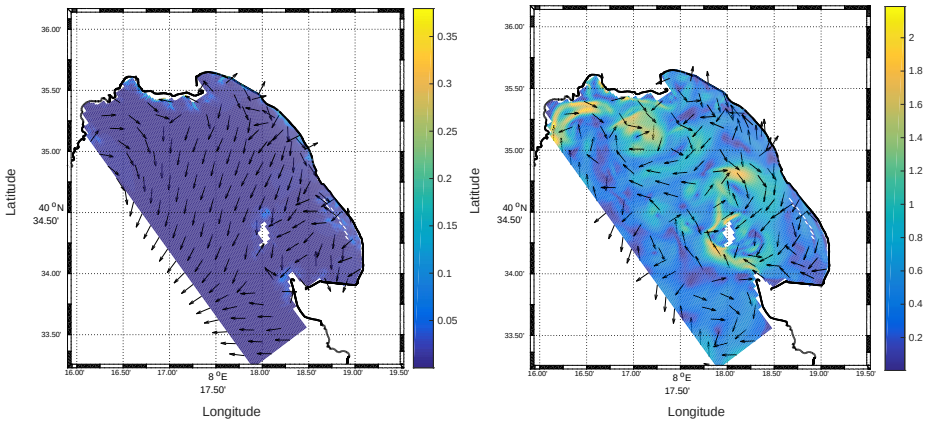

Figure 11: Norm (color map) and direction (arrows) of the depth-averaged velocity at the beginning of the simulation (left panel) and at the time of maximum wave height in the domain (right panel). The shoreline is also shown (black line).

Both x_s and z_s refer to the local still water shoreline position, i.e. $x_s = z_s = 0$ at time $t = 0$.

The Northern area (Figure 12) experiences larger inundations (x_s up to about 45m) and runup values (z_s up to about 1.5m), while the Southern area (Figure 13) is well protected by the emerged structures (maximum x_s and z_s being less than, respectively, 20m and 0.5m). In addition, due to the particular topography in the Northern area, the largest x_s occur at specific y locations (e.g., $y = 150$m), where a sort of channels exists between the more elevated regions (light red versus dark red areas in Figure 7), hence facilitating the water propagation landwards.

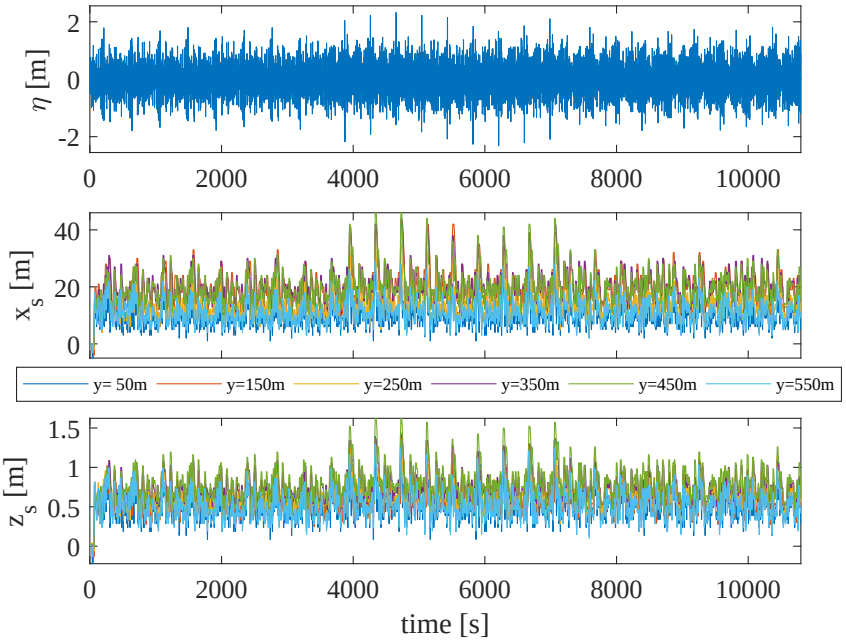

Figure 12: Water surface level at the offshore boundary (top panels), horizontal shoreline evolution x_s (middle panels) and vertical evolution z_s (bottom panels) for the Northern area. ROMS-SWAN-derived forcing.

The Northern area is characterized by some wave setup since the simulation start, as a consequence of the intense forcing and to the free-from-obstacle beach, hence the shoreline oscillates around $x_s = (10 - 15)$m and $x_s = (0.5 - 0.7)$m. Conversely, the Southern area is characterized by a shoreline oscillation around $x_s = z_s = 0$, this moving back and forth with respect to the still water shoreline, due to the wave-breakwater interaction. Hence, due to a small momentum flux and an almost null wave setup inshore of emerged structures (e.g., see Hughes, 2004; Lorenzoni et al., 2016), a reduced runup occurs in the protected Southern beach.

In Figure 14 the shoreline location at the beginning of the simulation (solid line), hence accounting for the imposed superelevation, and the line of maximum inundation after three hours (dashed line) are superposed to the North (left) and South (right) bathymetries. The maximum inundation line has been obtained in the post-processing by taking as flooded only the areas that are characterized by a minimum water depth of $d_{flood} = 10$cm, which is different from the minimum depth used for the wet-and-dry technique during the simulation, i.e. $d_{min} =$ 1mm (see Section 2.5). The use of such d_{flood} is consistent with the risk analysis that can be carried out on the studied zone. In addition, the illustrated results refer to the maximum inundation obtained from the analysis of 108 outputs,

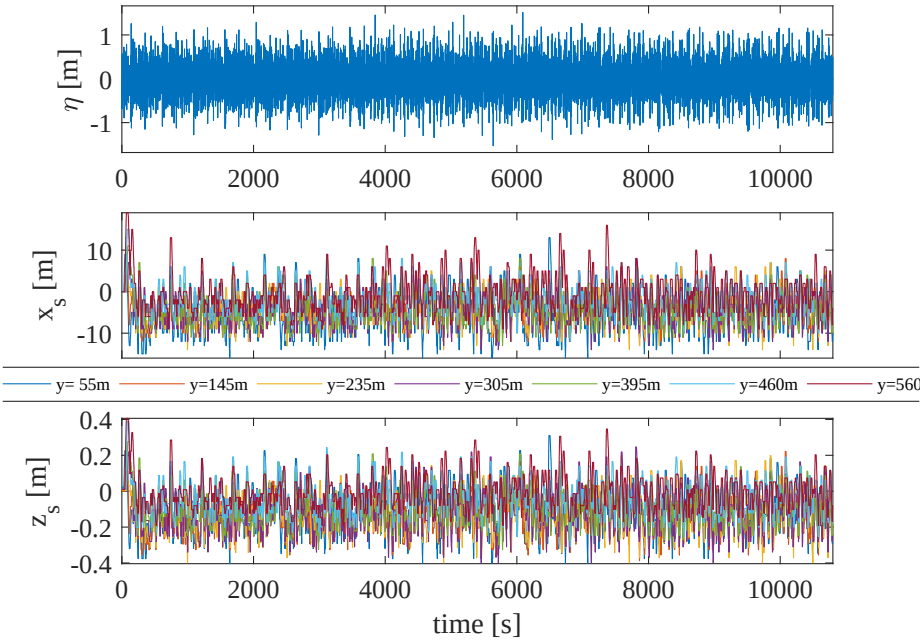

Figure 13: Water surface level at the offshore boundary (top panels), horizontal shoreline evolution x_s (middle panels) and vertical evolution z_s (bottom panels) for the Southern area. ROMS-SWAN-derived forcing.

i.e. one every 100s simulation.

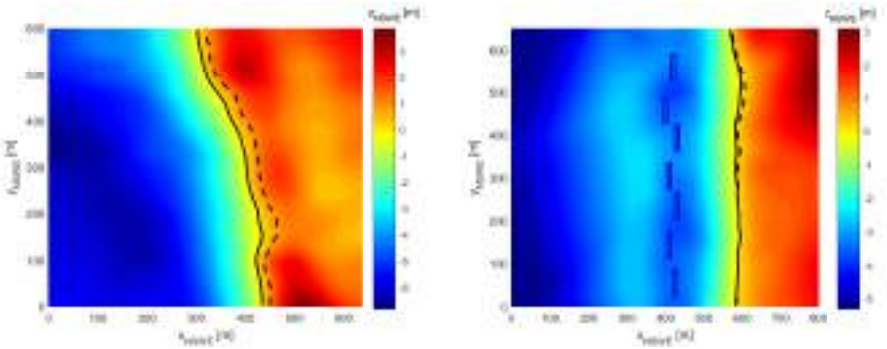

Figure 14: Inundation of the Northern (left) and Southern (right) regions obtained using the ROMS-SWAN forcing after 3 hours. The initial shoreline (black solid line), including the superelevation contribution, and the maximum inundation line (black dashed line) are also illustrated.

As already mentioned, some critical zones are characterized by a larger in-

undation, e.g., in the Northern area, at $y_{NSWE} = (140 - 190)$m (left panel of Figure 14), due to the presence of a lower-elevation zone. Here, the maximum inundation with respect to the initial shoreline is $x_s > 40$m. Conversely, the Southern area is much more protected by the breakwaters, hence the shoreline inundation $x_s < 20$m, also at $y_{NSWE} \cong 500$m, where the flooded area is larger [3].

4.3. NSWE forced by Go10's model

The same gauges used for the ROMS-SWAN-forced simulations have been placed within the domain. Similarly to what described in Section 4.2, Figures 15 and 16 illustrate the water surface at the boundary η (top panels), inundation x_s (middle panels), and runup z_s (bottom panels). Also in this case, the Northern area (Figure 15) experiences larger inundations ($x_s > 60$m) if compared to the Southern area (Figure 16), where the inundation is much smaller ($x_s < 45$m).

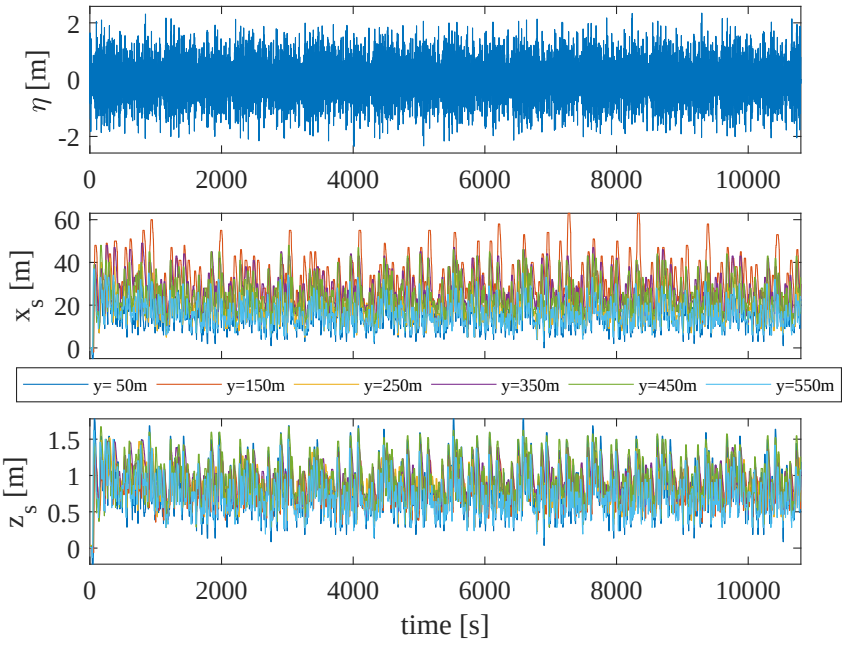

Figure 15: Water surface level at the offshore boundary (top panels), horizontal shoreline evolution x_s (middle panels) and vertical evolution z_s (bottom panels) for the Northern area. Go10's model-derived forcing.

Figure 17 shows that the maximum inundation line (dashed line) is much farther away from the initial shoreline location (solid line), if compared to the

[3] e.g., see http://www.algheroeco.com/mareggiata-ad-alghero-si-contano-danni/

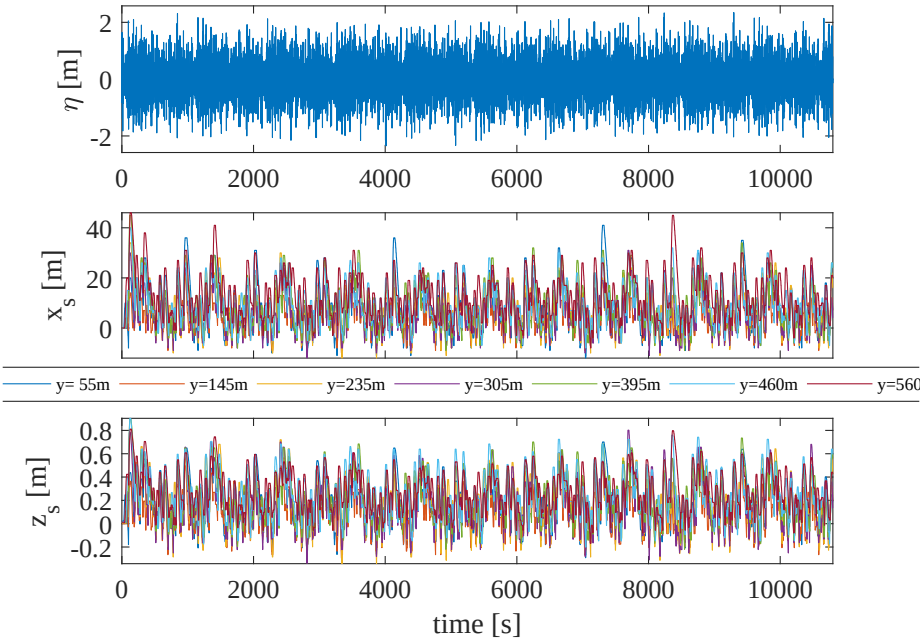

Figure 16: Water surface level at the offshore boundary (top panels), horizontal shoreline evolution x_s (middle panels) and vertical evolution z_s (bottom panels) for the Southern area. Go10's model-derived forcing.

results obtained with the ROMS-SWAN forcing. This happens for both North (left) and South (right) bathymetries. In the Northern domain, in addition to the above-mentioned critical zone ($y_{NSWE} = (140 - 190)$m), where $x_s \cong 60$m, another location results significantly prone to inundation, i.e. $y_{NSWE} = (350 - 400)$m, where $x_s > 45$m. The Southern area is more protected, but the larger waves forced using Go10's model, provide inundations up to 48m at $y_{NSWE} = (0 - 20)$m, where the breakwater protection is reduced, while it is $x_s \cong 35$m in a more protected zone, i.e. at $y_{NSWE} = (500 - 550)$m.

With the aim to better clarify how the results of Figures 14 and 17 have been retrieved, an example is provided in the present section. The maximum inundation line represents the envelope of all wave runups obtained during the 3-hour simulations, with outputs every 100s. In particular, at each y_{NSWE} coordinate, the maximum x_s has been calculated among the 108 available outputs, so as to obtain the final maximum inundation line. As an example, Figure 18 illustrates the evolution of the shoreline time series (colored thin lines) and the maximum inundation line (thick green line) at the Southern region.

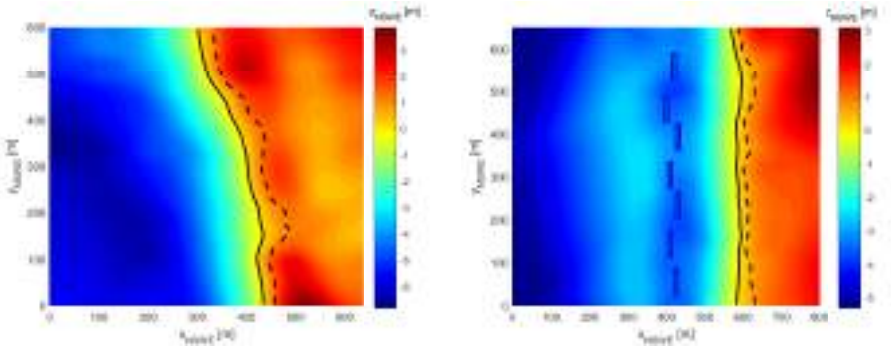

Figure 17: Inundation of the Northern (left) and Southern (right) regions obtained using Go10's model forcing after 3 hours. The initial shoreline (black solid line), including the superelevation contribution, and the maximum inundation line (black dashed line) are also illustrated.

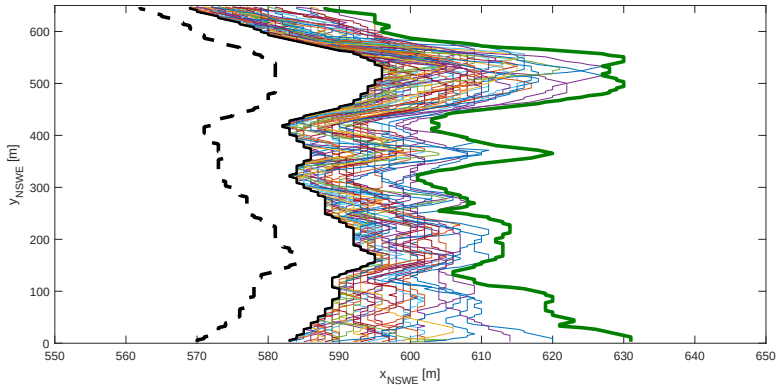

Figure 18: Example of maximum inundation line (thick green line) at the Southern region after the 3-hour Go10's simulation. The envelope has been obtained from the 108 shorelines (colored thin lines) extracted every 100s from the simulation. The initial shoreline (black solid line) and the still water shoreline (black dashed line) are also illustrated.

4.4. Comparison

The results of both simulation types are illustrated for the Northern (Figure 19) and Southern (Figure 20) areas. Since a fixed superelevation ($\Delta\eta_{tot}$) has been imposed to the whole domain, the initial shoreline is shifted landward with respect to the still water shoreline of about $(10 - 15)$m. Hence, in addition to the initial shoreline (black solid line), which accounts for the superelevation, the still-water shoreline is represented (black dashed line), to better compare the wave runup and flooding during the sea storm with respect to calm conditions. The maximum inundation lines obtained using ROMS-SWAN (blue lines) and Go10's model (green lines) are also reported.

The shoreline retreat, i.e. the distance between the still water shoreline and

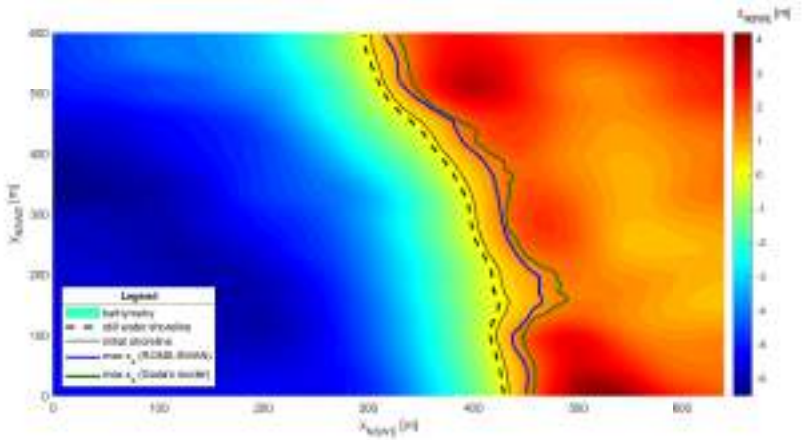

Figure 19: Inundation of the Northern region: comparison between the maximum inundation obtained using the ROMS-SWAN forcing (blue line) and Go10's model forcing (green line) after 3 hours. The initial shoreline (black solid line) and the still water shoreline (black dashed line) are also illustrated.

the maximum x_s, at location $y_{NSWE} = 159$m of the Northern area is about 42m and 67m for, respectively, the ROMS-SWAN case and the Go10's model case. Further, at $y_{NSWE} = 360$m, the shoreline retreat is 37m and 55m when, respectively, either the ROMS-SWAN or Go10's model forcing is used.

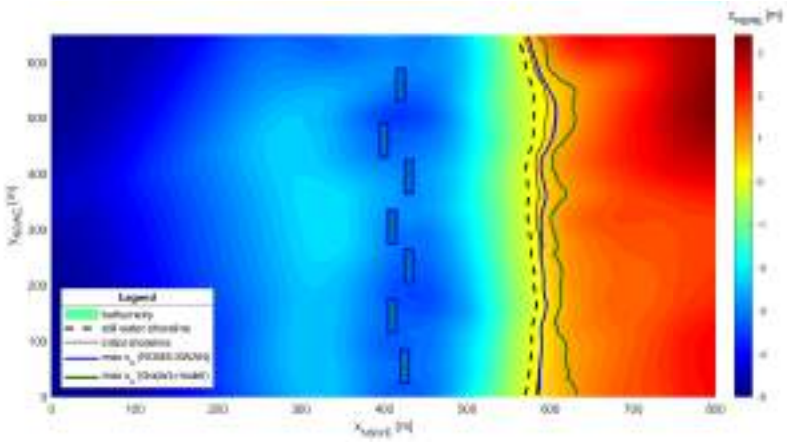

Figure 20: Inundation of the Southern region: comparison between the maximum inundation obtained using the ROMS-SWAN forcing (blue line) and Go10's model forcing (green line) after 3 hours. The initial shoreline (black solid line) and the still water shoreline (black dashed line) are also illustrated.

The Southern simulations are characterized by a shoreline retreat, at $y_{NSWE} = 3$m, of 16m (ROMS-SWAN) and 61m (Go10's model), while at $y_{NSWE} = 548$m,

the retreat is 20m (ROMS-SWAN) and 50m (Go10's model). Hence, the difference between the inundation results obtained from the two simulation typologies is, at most, of the order of $(20-30)$m in the Northern area, while such difference is 45m in the Southern region.

This demonstrates that the used analytical model properly captures the wave characteristics to be used to feed the NSWE solver, but is significantly conservative if compared to the results obtained using a forcing coming from a phase-averaged model. This can also be due to the breaking coefficients used by Go10, which are too small, especially in the presence of very mildly sloping beaches (e.g., see Allsop et al., 1998).

Finally, a comparison has been attempted with two of the most common formulas used for the runup prediction, i.e. those by Stockdon et al. (2006). A foreshore slope ranging between $s_f = 1/40$ and $s_f = 1/20$ has been assumed, while as offshore wave characteristics, those used for the application of Go10's approach (see Table 1) have been applied. The 2% runup predicted by Stockdon et al. (2006)'s general law is $R_{2\%} = (1.07 - 1.40)$m. The other law, valid for dissipative beaches, i.e. characterized by an Iribarren number $\xi_0 < 0.3$ (like in the present case), gives $R_{2\%} = 1.01$m, independently of the slope. While the latter value significantly underestimates the results obtained using Go10's approach on the free beach, the general formula applied to the steepest part of the beach ($s_f = 1/20$) gives $R_{2\%} = 1.40$m, i.e. only slightly underestimates the maximum simulated runup, which is $z_s = 1.58$m (see Figure 17).

5. Conclusions

A model chain methodology to estimate the maximum beach inundation has been illustrated. Approaches of this kind are fundamental inputs for the risk analysis of coastal regions, hence can significantly support the decision-making process related to both mitigation strategies, aimed at defending the coast from flooding, and further implications of socio-economic and environmental nature.

The proposed methodology exploits a modeling chain, which starts from an offshore datum, moves to the offshore-nearshore wave propagation, and ends with the wave propagation up to the shore. The use of such a modeling chain allows to: 1) fully exploit the main different characteristics of each sub-model, which is specifically tailored for a given task at the needed resolution, 2) give proper account of the whole range of physical processes that evolve while approaching the coastline from offshore.

The offshore datum can be provided by either a device (e.g., a buoy) or a forecasting system, while the offshore-nearshore wave propagation can be accomplished using a wave-averaged rather than an analytical model. The final part, i.e. the beach-inundation prediction, is undertaken through a wave-resolving model.

In the present work, the first link of the chain is represented by the Kassandra system, the second link by either the ROMS-SWAN model or Goda (2010)'s model, the third by the NSWE model. To demonstrate the feasibility of the proposed methodology, an application has been illustrated using the

above tools, and the Alghero bay (Sardinia, Italy) has been chosen for such an application. After a specific treatment of both available wave data and bathymetric surveys, the wave propagation, through either the phase-averaged or the analytical model, has provided useful information (boundary conditions) to run the phase-resolving model, which, in turn, has provided the final beach inundation in two regions. In particular, the use of the analytical model has provided largest flooded areas, especially in the Southern region, characterized by a less sloping beach and protected by emerged breakwaters.

Hence, the proposed methodology has been found to be suitable for the analysis of the coastal flooding, and the real-world application confirmed that, for the wave propagation from the offshore to the nearshore, simplified (analytical) models may lead to inundation results similar to those obtained using more complete (numerical) models, in terms of order of magnitude $O(10)$m. Conversely, for a coastal risk analysis and hazard mapping purposes, differences due to the use of an analytical rather than a wave-averaged model could be substantial, with up to $(40-50)$m in the horizontal direction and $(40-50)$cm in the vertical direction, hence this should be taken into due account.

Acknowledgments

The present work is supported by the project titled "*Ricerca dei fenomeni e pertinenti effetti delle inondazioni costiere volti allindividuazione di una metodologia di studio e approfondimento della pericolosit di inondazione marina attraverso lindividuazione di linee guida e criteri duso compatibili con lattuale stato di pericolosit e di rischio dei luoghi senza incrementi di tali stati*", funded by the "Istituto Superiore per la Protezione e la Ricerca Ambientale" (ISPRA). We thank the Regione Sardegna for having made available some of the data used in our simulations. We also thank Dr. Marco Bajo, CNR-ISMAR, for part of the preprocessing on Kassandra dataset. Special thanks go to Dr. John Warner of the USGS, for the help provided in the use of the ROMS-SWAN system and for the many useful comments and suggestions given during the writing of the paper.

References

Allsop, N., Durand, N., Hurdle, D.. Influence of steep seabed slopes on breaking waves for structure design. Coastal Engineering Proceedings 1998;1(26).

Antuono, M., Brocchini, M.. Beyond boussinesq-type equations: semi-integrated models for coastal dynamics. Physics of Fluids 2013;25(1):016603.

Antuono, M., Colicchio, G., Lugni, C., Greco, M., Brocchini, M.. A depth semi-averaged model for coastal dynamics. Physics of Fluids 2017;29(5):056603.

APAT, . Atlante delle Coste Italiane Agenzia Protezione Ambiente e Territorio. Technical Report; APAT; 2006. In Italian.

Barcikowska, M.J., Weaver, S.J., Feser, F., Russo, S., Schenk, F., Stone, D.A., Wehner, M.F., Zahn, M.. Euro-atlantic winter storminess and precipitation extremes under 1.5 c vs. 2 c warming scenarios. Earth System Dynamics 2018;9(2):679.

Boccotti, P.. A general theory of three-dimensional wave groups part i: the formal derivation. Ocean engineering 1997;24(3):265–280.

Booij, N., Ris, R., Holthuijsen, L.H.. A third-generation wave model for coastal regions: 1. model description and validation. Journal of geophysical research: Oceans 1999;104(C4):7649–7666.

Briganti, R., Dodd, N., Kelly, D., Pokrajac, D.. An efficient and flexible solver for the simulation of the morphodynamics of fast evolving flows on coarse sediment beaches. International Journal for Numerical Methods in Fluids 2012;69(4):859–877.

Briganti, R., Torres-Freyermuth, A., Baldock, T.E., Brocchini, M., Dodd, N., Hsu, T.J., Jiang, Z., Kim, Y., Pintado-Patiño, J.C., Postacchini, M.. Advances in numerical modelling of swash zone dynamics. Coastal Engineering 2016;115:26–41.

Brocchini, M., Bernetti, R., Mancinelli, A., Albertini, G.. An efficient solver for nearshore flows based on the waf method. Coastal Engineering 2001;43(2):105–129.

Cavaleri, L., Alves, J.H., Ardhuin, F., Babanin, A., Banner, M., Belibassakis, K., Benoit, M., Donelan, M., Groeneweg, J., Herbers, T., et al. Wave modelling–the state of the art. Progress in oceanography 2007;75(4):603–674.

CCCuk, . UK Climate Change Risk Assessment 2017. Synthesis report: priorities for the next five years. UK Climate Change Risk Assessment 2017 Synthesis Report of Committee on Climate Change. Technical Report; 2016.

Corbella, S., Stretch, D.. Multivariate return periods of sea storms for coastal erosion risk assessment. Natural Hazards and Earth System Sciences 2012;12(8):2699–2708.

De Girolamo, P., Di Risio, M., Beltrami, G., Bellotti, G., Pasquali, D.. The use of wave forecasts for maritime activities safety assessment. Applied Ocean Research 2017;62:18–26.

De Leo, F., Besio, G., Zolezzi, G., Bezzi, M.. Coastal vulnerability assessment: through regional to local downscaling of wave characteristics along the bay of lalzit (albania). Natural Hazards and Earth System Sciences Discussions 2018;.

Di Risio, M., Bruschi, A., Lisi, I., Pesarino, V., Pasquali, D.. Comparative analysis of coastal flooding vulnerability and hazard assessment at national scale. Journal of Marine Science and Engineering 2017;5(4):51.

Ferrarin, C., Roland, A., Bajo, M., Umgiesser, G., Cucco, A., Davolio, S., Buzzi, A., Malguzzi, P., Drofa, O.. Tide-surge-wave modelling and forecasting in the mediterranean sea with focus on the italian coast. Ocean Modelling 2013;61:38–48.

Goda, Y.. Random seas and design of maritime structures. volume 33. World Scientific Publishing Company, 2010.

Guizien, K., Barthélemy, E.. Accuracy of solitary wave generation by a piston wave maker. journal of hydraulic research 2002;40(3):321–331.

Haas, K.A., Warner, J.C.. Comparing a quasi-3d to a full 3d nearshore circulation model: Shorecirc and roms. Ocean Modelling 2009;26(1-2):91–103.

Haidvogel, D.B., Arango, H., Budgell, W.P., Cornuelle, B.D., Curchitser, E., Di Lorenzo, E., Fennel, K., Geyer, W.R., Hermann, A.J., Lanerolle, L., et al. Ocean forecasting in terrain-following coordinates: Formulation and skill assessment of the regional ocean modeling system. Journal of Computational Physics 2008;227(7):3595–3624.

Heidari, A.. Structural master plan of flood mitigation measures. Natural Hazards and Earth System Sciences 2009;9(1):61–75.

Helman, P., Tomlinson, R.. Two centuries of climate change and climate variability, east coast australia. Journal of Marine Science and Engineering 2018;6(1):3.

Holthuijsen, L.H.. Waves in oceanic and coastal waters. Cambridge University Press, 2010.

Hughes, S.A.. Estimation of wave run-up on smooth, impermeable slopes using the wave momentum flux parameter. Coastal Engineering 2004;51(11-12):1085–1104.

Inghilesi, R., Orasi, A., Catini, F.. The ispra mediterranean coastal wave forecasting system: evaluation and perspectives. Journal of Operational Oceanography 2016;9(sup1):s89–s98.

Kennedy, A.B., Chen, Q., Kirby, J.T., Dalrymple, R.A.. Boussinesq modeling of wave transformation, breaking, and runup. i: 1d. Journal of waterway, port, coastal, and ocean engineering 2000;126(1):39–47.

Liu, Z., Frigaard, P.. Generation and analysis of random waves 1999;.

Lorenzoni, C., Postacchini, M., Brocchini, M., Mancinelli, A.. Experimental study of the short-term efficiency of different breakwater configurations on beach protection. Journal of Ocean Engineering and Marine Energy 2016;2(2):195–210.

Lyard, F., Lefevre, F., Letellier, T., Francis, O.. Modelling the global ocean tides: modern insights from fes2004. Ocean dynamics 2006;56(5-6):394–415.

Ma, G., Shi, F., Kirby, J.T.. Shock-capturing non-hydrostatic model for fully dispersive surface wave processes. Ocean Modelling 2012;43:22–35.

Malguzzi, P., Grossi, G., Buzzi, A., Ranzi, R., Buizza, R.. The 1966 century flood in italy: A meteorological and hydrological revisitation. Journal of Geophysical Research: Atmospheres 2006;111(D24).

Manca, E., Cáceres, I., Alsina, J., Stratigaki, V., Townend, I., Amos, C.. Wave energy and wave-induced flow reduction by full-scale model posidonia oceanica seagrass. Continental Shelf Research 2012;50:100–116.

Manca, E., Pascucci, V., Deluca, M., Cossu, A., Andreucci, S.. Shoreline evolution related to coastal development of a managed beach in alghero, sardinia, italy. Ocean & coastal management 2013;85:65–76.

Mentaschi, L., Besio, G., Cassola, F., Mazzino, A.. Performance evaluation of wavewatch iii in the mediterranean sea. Ocean Modelling 2015;90:82–94.

Pala, D., Cossu, A.V.L., Pischedda, E., Pascucci, V., Andreucci, S., Ragazzola, F., Demelas, S., Sechi, N.. Indagini preliminari su ripartizione e morfologia della prateria a posidonia oceanica nella rada di alghero. Biol Mar Mediterr 2009;16(1):286–287. In Italian.

de la Peña, J., Sanchez, J., Diaz, R., Martin, M.. Physical model and revision of theoretical runup. Coastal Engineering Proceedings 2012;1(33):22.

Perini, L., Calabrese, L., Salerno, G., Ciavola, P., Armaroli, C.. Evaluation of coastal vulnerability to flooding: comparison of two different methodologies adopted by the emilia-romagna region (italy). Natural Hazards and Earth System Sciences 2016;16(1):181–194.

Postacchini, M., Brocchini, M.. A wave-by-wave analysis for the evaluation of the breaking-wave celerity. Applied Ocean Research 2014;46:15–27.

Postacchini, M., Russo, A., Carniel, S., Brocchini, M.. Assessing the hydromorphodynamic response of a beach protected by detached, impermeable, submerged breakwaters: a numerical approach. Journal of Coastal Research 2016;32(3):590–602.

Roeber, V., Cheung, K.F., Kobayashi, M.H.. Shock-capturing boussinesq-type model for nearshore wave processes. Coastal Engineering 2010;57(4):407–423.

Russo, A., Carniel, S., Benetazzo, A.. Support for iczm and msp in the adriatic sea region. Sea Technol 2013;54(8):27–35.

Salecker, D., Gruhn, A., Schlamkow, C., Fröhle, P.. Statistical analysis of hydrodynamic impacts for risk assessment of coastal areas. J Coastal Res, SI 2011;64:1906–1910.

Shchepetkin, A.F., McWilliams, J.C.. The regional oceanic modeling system (ROMS): A split-explicit, free-surface, topography-following-coordinate oceanic model. Ocean Modelling 2005;9(4):347–404. doi:10.1016/j.ocemod.2004.08.002.

Shchepetkin, A.F., McWilliams, J.C.. Correction and commentary for "Ocean forecasting in terrain-following coordinates: Formulation and skill assessment of the regional ocean modeling system" by Haidvogel et al., J. Comp. Phys. 227, pp. 3595-3624. Journal of Computational Physics 2009;228(24):8985–9000. doi:10.1016/j.jcp.2009.09.002.

Soldini, L., Antuono, M., Brocchini, M.. Numerical modeling of the influence of the beach profile on wave run-up. Journal of Waterway, Port, Coastal, and Ocean Engineering 2012;139(1):61–71.

Stockdon, H.F., Holman, R.A., Howd, P.A., Sallenger Jr, A.H.. Empirical parameterization of setup, swash, and runup. Coastal engineering 2006;53(7):573–588.

Svendsen, I., Madsen, P., Hansen, J.B.. Wave characteristics in the surf zone. Coastal Engineering Proceedings 1978;1(16).

Thompson, P., Cai, Y., Reeve, D., Stander, J.. Automated threshold selection methods for extreme wave analysis. Coastal Engineering 2009;56(10):1013–1021.

Villatoro, M., Silva, R., Méndez, F., Zanuttigh, B., Pan, S., Trifonova, E., Losada, I., Izaguirre, C., Simmonds, D., Reeve, D., et al. An approach to assess flooding and erosion risk for open beaches in a changing climate. Coastal Engineering 2014;87:50–76.

Warner, J.C., Armstrong, B., He, R., Zambon, J.B.. Development of a Coupled Ocean-Atmosphere-Wave-Sediment Transport (COAWST) Modeling System. Ocean Modelling 2010;35(3):230–244. doi:10.1016/j.ocemod.2010.07.010.

Weisse, R., Bellafiore, D., Menéndez, M., Méndez, F., Nicholls, R.J., Umgiesser, G., Willems, P.. Changing extreme sea levels along european coasts. Coastal engineering 2014;87:4–14.

Zampato, L., Bajo, M., Canestrelli, P., Umgiesser, G.. Storm surge modelling in venice: two years of operational results. Journal of Operational Oceanography 2016;9(sup1):s46–s57.

Zitti, G., Ancey, C., Postacchini, M., Brocchini, M.. Impulse waves generated by snow avalanches: momentum and energy transfer to a water body. Journal of Geophysical Research: Earth Surface 2016;121(12):2399–2423.